Flexosensitive polarization vortices in thin ferroelectric films

Anna N. Morozovska,[1] Eugene A. Eliseev,[2] Sergei V. Kalinin,[3,*] and Riccardo Hertel[4,†]

[1]*Institute of Physics, National Academy of Sciences of Ukraine, 46, pr. Nauky, 03028 Kyiv, Ukraine*

[2]*Institute for Problems of Materials Science, National Academy of Sciences of Ukraine, Krjijanovskogo 3, 03142 Kyiv, Ukraine*

[3]*Center for Nanophase Materials Sciences, Oak Ridge National Laboratory, Oak Ridge, 37831 Tennessee, USA*

[4]*Université de Strasbourg, CNRS, Institut de Physique et Chimie des Matériaux de Strasbourg, UMR 7504, 67000 Strasbourg, France*

(Received 15 May 2021; revised 23 July 2021; accepted 2 August 2021; published 18 August 2021)

We present a theoretical study on the influence of the flexoelectric coupling on the spatial distribution and temperature behavior of the spontaneous polarization for several types of stable domain structure in thin ferroelectric films, such as stripe domains and vortices. Finite-element modeling (FEM) for $BaTiO_3$ films and analytical calculations within the Landau-Ginzburg-Devonshire approach reveals that an out-of-plane polarization component can be very sensitive to the flexoelectric coupling for periodic quasi-2D stripe domains and 3D vortex-antivortex structures. However, the influence is rather different for these structures. The flexoelectric coupling increases significantly the amplitude of a small out-of-plane polarization component in the stripe domains, and the "up" or "down" direction of the component is defined by the sign of the flexoelectric coefficients. Concerning the vortex-antivortex pairs, their antivortices with in-plane anticirculation have smooth wide dipolar cores through the entire film, whose shape and other features are almost insensitive to the coupling. The vortices with in-plane vorticity have spikelike cores with an out-of-plane quadrupolar moment induced by the flexoelectric coupling. The cores are located near the film–dead-layer interfaces. FEM results corroborated by analytical calculations prove that a change of the flexoelectric coefficient sign leads to a reorientation of the core axial polarization, making the flexosensitive 3D vortices similar to the recently introduced "flexons" in cylindrical nanoparticles. The relatively wide temperature range (from 200 to 400 K) of the flexosensitive vortices' existence gives us confidence that they can be observed experimentally in thin ferroelectric films by scanning-probe and nonlinear optical microscopy methods.

DOI: 10.1103/PhysRevB.104.085420

I. INTRODUCTION

Since its appearance and until now, nanoscale ferroics (ferromagnets, ferroelectrics, ferroelastics) have been one of the main subjects of fundamental research on the physical nature of long-range order of polar, magnetic, and structural properties [1–3]. The leading role is played by the emergence of a domain structure of long-range order parameters, such as electric polarization, magnetization, and (anti)ferrodistortion, and its interaction with the surface of a nanoferroic [4,5]. In the case of ferroelectrics, which we discuss here, the long-range order of the domains is governed by both electrostatic fields and the distribution of strain fields and their gradients. A strong and spatially extended gradient of elastic fields generated by the surface, domain walls, and/or other inhomogeneities can create a sizable flexoelectric polarization, which is proportional to this gradient (this phenomenon is a direct flexoelectric effect) [6]. On the other hand, the electrical polarization gradient gives rise to an inhomogeneous strain (inverse flexoelectric effect) [7]. The thermodynamic description of the flexoelectric effect is given by Lifshitz invariants [8,9].

The flexoelectric effect exists in all ferroics [6–9], in contrast to the flexomagnetic [10] and flexomagnetoelectric [11,12] effects, the existence of which is critically sensitive to the presence of time inversion and its connection with other operations of point symmetry of a particular material [13,14]. The influence of the flexoelectric effect on the macroscopic properties of ferroics (as well as any other materials) is relatively small [6–9]. However, in nanosized and nanostructured ferroics, the influence of the flexoelectric effect on their polar, magnetic, electronic properties and phase transitions can be significant, and it may lead to fundamental changes in their properties [15–17]. This size dependence of the effect arises from the gradients of physical quantities playing a leading role in such nanosystems [18,19].

Recently, it was predicted theoretically that a decrease in the correlation-gradient polarization energy leads to a significant increase in the polarization gradient, which in turn leads to spontaneous bending of otherwise uncharged domain walls in thin multiferroic films [20] and ferroelectric nanoparticles [21]. Such domain walls can form meandering [20] and/or labyrinthine [21] structures. Later, similar structures were discovered experimentally in thin $BiFeO_3$ and $Pb(Zr_{0.4}Ti_{0.6})O_3$ films by high resolution scanning transmission electron microscopy [22] and Piezoelectric Force Microscopy (PFM) [23] methods, respectively, and confirmed by *ab initio* calculations [23]. However, the influence of flexoeffects on the

*sergei2@ornl.gov

†riccardo.hertel@ipcms.unistra.fr

morphology of domain structures in thin films has not yet been studied systematically.

Most published experimental studies of flexoelectric phenomena in proper [24–26] and incipient [27,28] ferroelectrics, atomistic quantum-mechanical [29,30] and first-principles calculations [31–34] are overwhelmingly aimed at determining the magnitude of the flexoelectric coefficients [28–34] and the structure of the flexoelectric tensor [35,36]. The majority of the phenomenological papers on this topic are devoted to the influence of the flexoeffects on the macroscopic properties and phase transitions of the ferroic film as a whole (see, e.g., Refs. [37–39] and references therein), and only a few of them address the actual influence of the flexoelectric effect on the structure of domain walls [40–44]. The main result of Refs. [40–44] is the prediction that the flexoelectric effect induces the appearance of a small but sufficiently strong polarization component perpendicular to the plane of the nominally uncharged domain wall of the ferroic, resulting in an effective "charging" of the wall. PFM and conduction Atomic force microscopy (cAFM) experiments registering the conductivity of nominally uncharged domain walls in ferroelectrics and multiferroics confirm the theoretical predictions [45–47]. Non-Ising and chiral ferroelectric domain walls have been revealed by nonlinear optical microscopy [48].

Note that only a few works analyzed the influence of the flexoelectric coupling on the curled vortexlike domain structures in ferroelectric thin films [49], nanodots [50], and nanoparticles [51,52]. Namely, using machine learning and phase-field modeling, Li *et al.* [49] analyzed the role of flexoelectricity on polar 2D vortices in a $PbTiO_3/SrTiO_3$ superlattice. The axis of these vortices is parallel to the film surface, and the flexoelectric coupling influenced their details in a quantitative way, but not sharply or critically. Liu *et al.* [50] revealed that an out-of-plane polarization component appears in the polarization vortex in $PbTiO_3$ nanodots due to the flexoelectric effect. The influence of flexoelectricity on polarization vortices in spherical [51] and cylindrical [52] core-shell ferroelectric nanoparticles can be significant because it can induce a small axial polarization of the vortex core. Analytical calculations and simulations [52] have proven that a change of the flexoelectric coefficient sign leads to a reorientation of the axial polarization of the vortex and that an anisotropy of the flexoelectric coupling critically influences the vortex-core formation and its related domain morphology. Here we consider the influence of the flexoelectric coupling on the spatial distribution and temperature behavior of the spontaneous polarization for several types of stable domain structures in thin $BaTiO_3$ films, such as periodic quasi-2D stripe domains and arrays of 3D vortex-antivortex pairs, whose axes are perpendicular to the film surface.

II. PROBLEM STATEMENT

Using finite-element modeling (FEM) and the Landau-Ginzburg-Devonshire (LGD) phenomenological approach combined with electrostatic equations and elasticity theory, we model the polarization, internal electric field, elastic stresses, and strains in a thin $BaTiO_3$ film. We consider a $BaTiO_3$ film [001] sandwiched between two ultrathin paraelectric dead layers with a high relative dielectric permittivity.

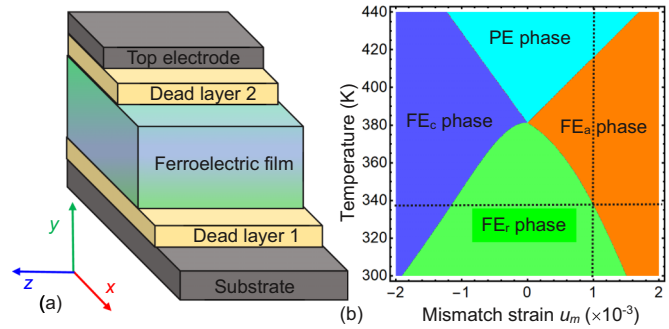

FIG. 1. (a) The ferroelectric film is placed between two paraelectric dead layers with a very high dielectric permittivity. The dead layers' thickness is 0.8 nm and the relative dielectric permittivity is 300. The mismatch strain exists at the interface "dead layer 1–conducting substrate." The coordinate frame we are using is shown in the bottom left corner. (b) Phase diagram of a thick single-domain $BaTiO_3$ film covered with perfect electrodes and placed on a rigid substrate. PE and FE denote the paraelectric and ferroelectric phases, respectively. Indices "*c*," "*r*," and "*a*" correspond to the tetragonal *c* phase with out-of-plane polarization; the rhombohedral phase comprising all three components of polarization; and the *a* phase with two in-plane components of polarization, respectively.

A top electrode and conducting substrate are in contact with the layers, and the voltage is applied between the conductors [see Fig. 1(a)]. The dead layers are required for the thermodynamic stability of the domain structure. Only a single-domain distribution is stable in the case of perfect electric contact between the ferroelectric film surfaces and ideal conducting electrodes. The film thickness varies from 4 to 20 nm, and the thickness of each dead layer varies from 0 to 0.8 nm. The relative dielectric permittivity is 300.

For most cases, we impose a slight tensile strain $0 < u_m < 0.25\%$ at the interface between the $BaTiO_3$ film and the substrate. The strain leads to the disappearance of the metastable orthorhombic phase and shifts the temperatures of the structural and polar transitions [53]. Also, the strain supports a rhombohedral ferroelectric phase in a single-domain film at temperatures below 360 K. At the same conditions, the formation of in-plane domains is favorable in the film due to depolarization effects. The transition from the rhombohedral to the tetragonal phase occurs at a temperature above 360 K, while the transition from the tetragonal ferroelectric to the paraelectric cubic phase occurs above 420 K [see Fig. 1(b)].

An LGD free-energy functional G of the $BaTiO_3$ film includes a Landau energy—an expansion on 2-4-6 powers of the polarization components P_i, G_{Landau}; a polarization gradient energy, G_{grad}; the electrostatic energy, G_{el}; an elastic, electrostriction contribution G_{es}; a flexoelectric contribution, G_{flexo}; and a surface energy term, G_S [37,39]. The free-energy functional, Landau-Khalatnikov equations [54,55], obtained from its variation, a mathematical formulation of the electrostatic and elastic subproblem, and FEM simulation details are given in Appendix A of Supplemental Material [56]. The ferroelectric, dielectric, and elastic properties of the $BaTiO_3$ [001] are listed in Table AI of Supplemental Material [56]. They are collected from Refs. [31,57].

For the initial distribution of the polarization in the film, we used either a periodic 90° zigzag pattern of in-plane domain stripes or a regular arrangement of crossed 90° domain walls in the XZ plane (see Figs. A1(a)–A1(c) in Appendix A of Supplemental Material [56]). When we used a purely random noise as the initial distribution of polarization at room temperature, it relaxed to in-plane a-domain stripes without any flux closure at the film surfaces. This circumstance can indicate that a-domain stripes are the energetic ground-state configuration for a film in the rhombohedral phase. In fact, the energy density of the periodic stripe domains is -1.560 MPa, while the energy density of the vortex-antivortex pairs is -1.373 MPa (for the same polarity of antivortex cores) or -1.368 MPa (for the opposite polarity of antivortex cores) for a 10-nm $BaTiO_3$ film at room temperature.

To study the influence of the flexoelectric coupling, we changed the signs of all components of the flexoelectric tensor F_{ij} simultaneously, e.g., we put $F_{11} \rightarrow -F_{11}$, $F_{12} \rightarrow -F_{12}$, $F_{44} \rightarrow -F_{44}$ for the considered case of $BaTiO_3$ with a cubic parent phase. In this work we changed the sign of all F_{ij} simultaneously because the relations between some of the components can be fixed by a concrete symmetry of the material (e.g., $F_{44} = F_{11} - F_{12}$ for an isotropic symmetry), while their magnitude and total sign is symmetry independent. Changing the signs and values of the components F_{ij} independently would be an interesting but very time-consuming task deserving a separate study.

III. FLEXOELECTRIC COUPLING INFLUENCE ON THE POLARIZATION DISTRIBUTION

Our FEM studies revealed that the out-of-plane polarization component P_y can be highly sensitive to the flexoelectric coupling (in short: "flexocoupling") for both stripe domains and vortices. However, the influence is rather different for each of them.

The influence of the flexocoupling on the in-plane periodic stripe domains in a 5-nm $BaTiO_3$ film is shown in Fig. 2. The dependence of the polarization magnitude $P = |\vec{P}|$ on F_{ij} is negligible, and thus Fig. 2(a) is the same for positive, zero, and negative F_{ij}. This happens because the value of P is governed by the in-plane polarization components, P_x and P_z, and the amplitude of P_x (about 20 $\mu C/cm^2$) is almost flexoinsensitive [see Fig. 2(e)]. Although the flexocoupling modulates the amplitude of P_z, the modulation amplitude is very small (less than 0.6 $\mu C/cm^2$) in comparison with its almost constant value $\sim$19 $\mu C/cm^2$ [see Fig. 2(g)]. The flexocoupling significantly increases the amplitude of a small out-of-plane polarization component P_y (from 0.1 to 0.4 $\mu C/cm^2$), and the up or down direction of P_y is defined by the sign of flexocoupling coefficients F_{ij}. The amplitude of P_y is proportional to the strength $|F_{ij}|$. This effect is illustrated qualitatively in Figs. 2(b), 2(c), and 2(d) for negative, zero, and positive F_{ij}, respectively. The quantitative influence of F_{ij} on P_y is clearly seen from z profiles of P_y in Fig. 2(f), which are calculated at the film top surface for negative (blue curves), zero (black curves), and positive (red curves) flexoelectric coefficients F_{ij}. Note that the small value of P_y at $F_{ij} = 0$ results from the electrostrictive coupling, and its phase depends on the initial conditions in the case.

We stress that the flexocoupling influence on P_i revealed in this work and shown in Fig. 2, is in qualitative agreement with earlier predictions about the flexocoupling-induced Néel polarization component at a "nominally uncharged" single domain wall in bulk rhombohedral $BaTiO_3$ [43] and $BiFeO_3$ [41]. However, the flexocoupling influence on the periodic stripe a domains in thin films is quantitatively different from that found in the case of single walls in a bulk rhombohedral material [41–43]. Using the results of Ref. [41], an approximate analytical expression for the Néel-type component

$$P_y \approx \frac{\varepsilon_0 \varepsilon_b f_Q}{1 + 2\beta\varepsilon_0\varepsilon_b} \frac{\partial P_x^2}{\partial z} + \frac{\varepsilon_0 \varepsilon_b q P_x}{1 + 2\beta\varepsilon_0\varepsilon_b} \left(P_s^2 - P_x^2\right), \quad (1)$$

can be used as an estimate in the vicinity of the domain walls. Here the first term has flexoelectric nature, and the second term originates from electrostriction coupling. Constants $f_Q \approx F_{12} \frac{Q_{11}s_{12} - s_{11}Q_{12}}{s_{11}^2 - s_{12}^2}$, $\beta \approx a_1 + (a_{12} + Q_{44}^2/2s_{44})P_s^2$, and $q \approx -\frac{Q_{11}s_{12} - s_{11}Q_{12}}{s_{11}^2 - s_{12}^2} Q_{44}$, where F_{12} is the flexoelectric coefficient, Q_{ij} are electrostriction coefficients, s_{12} are elastic compliances, a_1 and a_{12} are LGD expansion coefficients, P_s is the spontaneous polarization, ε_b is a background permittivity [58], and ε_0 is the vacuum permittivity (see Table AI [56]).

The influence of the flexocoupling on a periodic lattice of polarization vortices and antivortices is shown in Figs. 3–5 and Figs. B1–B3 [56] for a 9-nm $BaTiO_3$ film stretched with a misfit strain 0.1%. The computation cell, which translates periodically, is a rectangular parallelepiped consisting of two vortices separated by two antivortices (see Fig. 3 and Fig. B1). The vortex and antivortex can be topologically distinguished by the winding number $W = \oint \frac{\nabla\alpha(\varphi)}{2\pi} dS$, that is the normalized line integral on a closed loop S over the gradient of the angle $\alpha(\varphi)$ that the in-plane component of the polarization $\vec{P}$ encloses with the x axis [59,60]. The winding number counts the number of vortex ($W = +1$) and antivortex ($W = -1$) structures within the loop S [see Figs. 6(a)–6(c)].

Besides topological aspects, vortices and antivortices also differ concerning their energy. Although the correlation energy is similar in both cases, vortex structures are virtually divergence-free, such that they tend to form spontaneously in inhomogeneous structures to reduce the dipolar energy. By contrast, antivortices display strong divergences, leading to a distinct distribution of bound charges and a corresponding increase in dipolar energy. This behavior is known from magnetic structures, and the situation in ferroelectrics is analogous: here the divergence $div\ \vec{P}$ is relatively small in the vortex core case and quite significant in the antivortex one (see Fig. A1(d) in Appendix A [56]). Because of these differences in energy, individual antivortices tend to dissolve in magnetic systems, and particular geometric shapes are required to stabilize them [61]. Antivortex structures typically occur for topological reasons as they form a link between two neighboring vortices with equal circulation. In magnetic structures, such situations are well-known in the form of "cross-tie" domain walls [62], which are essentially linear chains of alternating vortex-antivortex structures. However, we are not aware of a generalization of cross-tie domain-wall structures

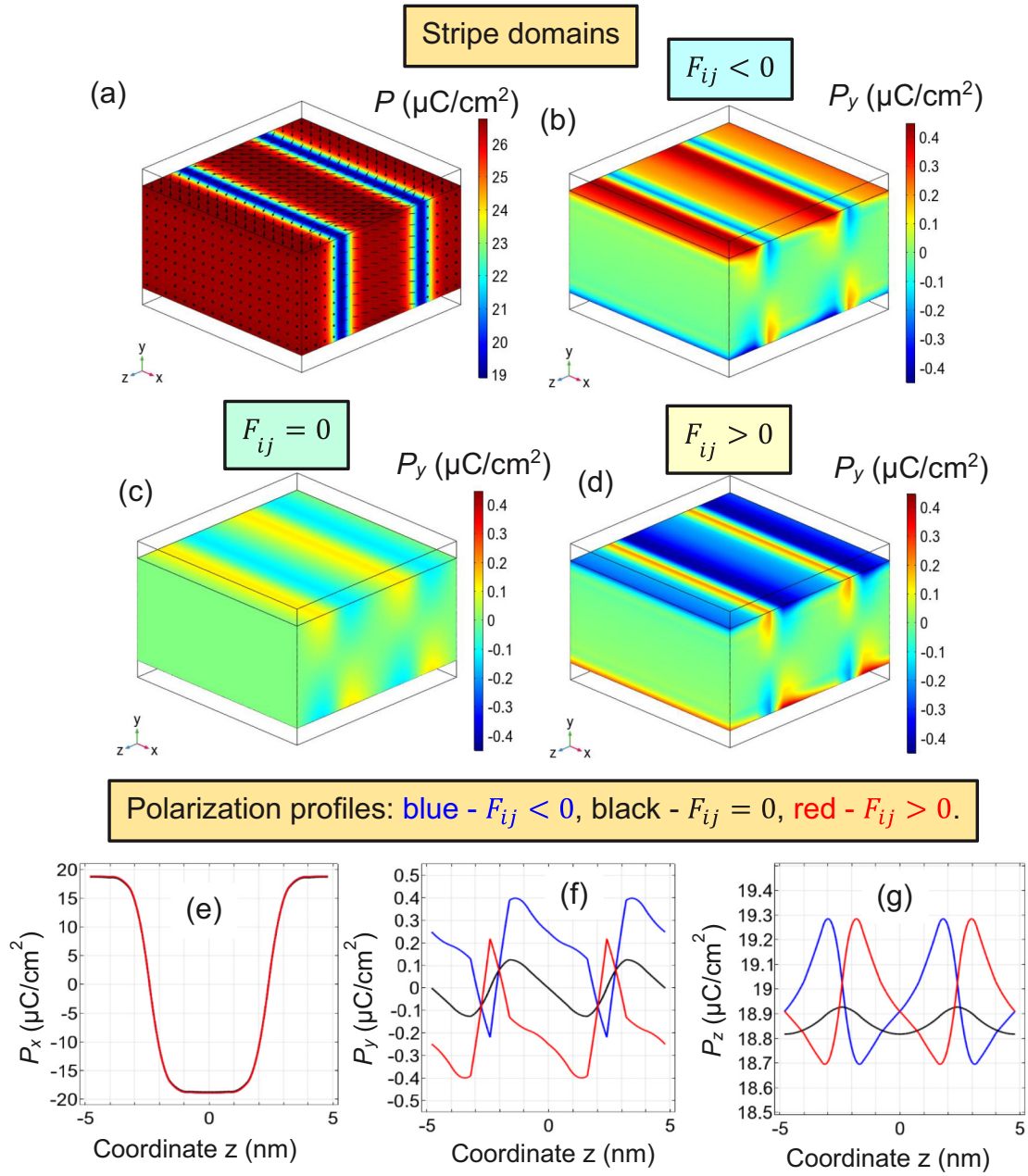

FIG. 2. Regular stripe domains inside a thin strained $BaTiO_3$ film. Polarization magnitude P (a) and out-of-plane component P_y calculated for negative (b), zero (c), and positive (d) flexoelectric coefficients F_{ij}. (e)–(g) Polarization z profiles calculated at the film top surface for negative (blue curves), zero (black curves), and positive (red curves) flexoelectric coefficients F_{ij}. The film thickness is 5 nm, mismatch strain $u_m = 0.2\%$, and the temperature T is 300 K. The dependence of P on F_{ij} is negligible and not shown in the figure. Arrows in the plot (a) show the direction of polarization vector.

to two-dimensional checkerboard-type vortex-antivortex arrays.

It appears that the dependence of the polarization magnitude P on F_{ij} is very weak, and so the images in Figs. 3(d) and 4(c), as well as P profiles shown in Figs. 5(a) and 5(b), are almost F_{ij} independent. In contrast to the magnitude, the distribution of the out-of-plane polarization component P_y does depend on F_{ij}, i.e., it is "flexosensitive," but the sensibility is only significant for a vortex region (as will be shown below).

The antivortex has a wide and smooth dipolar core, whose rounded rectangularlike shape and other features are weakly sensitive to the flexocoupling [see Figs. 3(a)–3(c) and Figs. B2(a)–B2(c)]. The direction of the component P_y in the antivortex core is defined by initial conditions [compare Figs. 4(a) and 4(b)], but not by the F_{ij} structure. The magnitude of P_y in the antivortex core is relatively high, reaching (10–15) $\mu C/cm^2$ for thin films [see Figs. 5(c), 5(e), and 5(g)].

The vortex has a very prolate asymmetrical spikelike quadrupolar core, whose polarity (which is defined by the sign

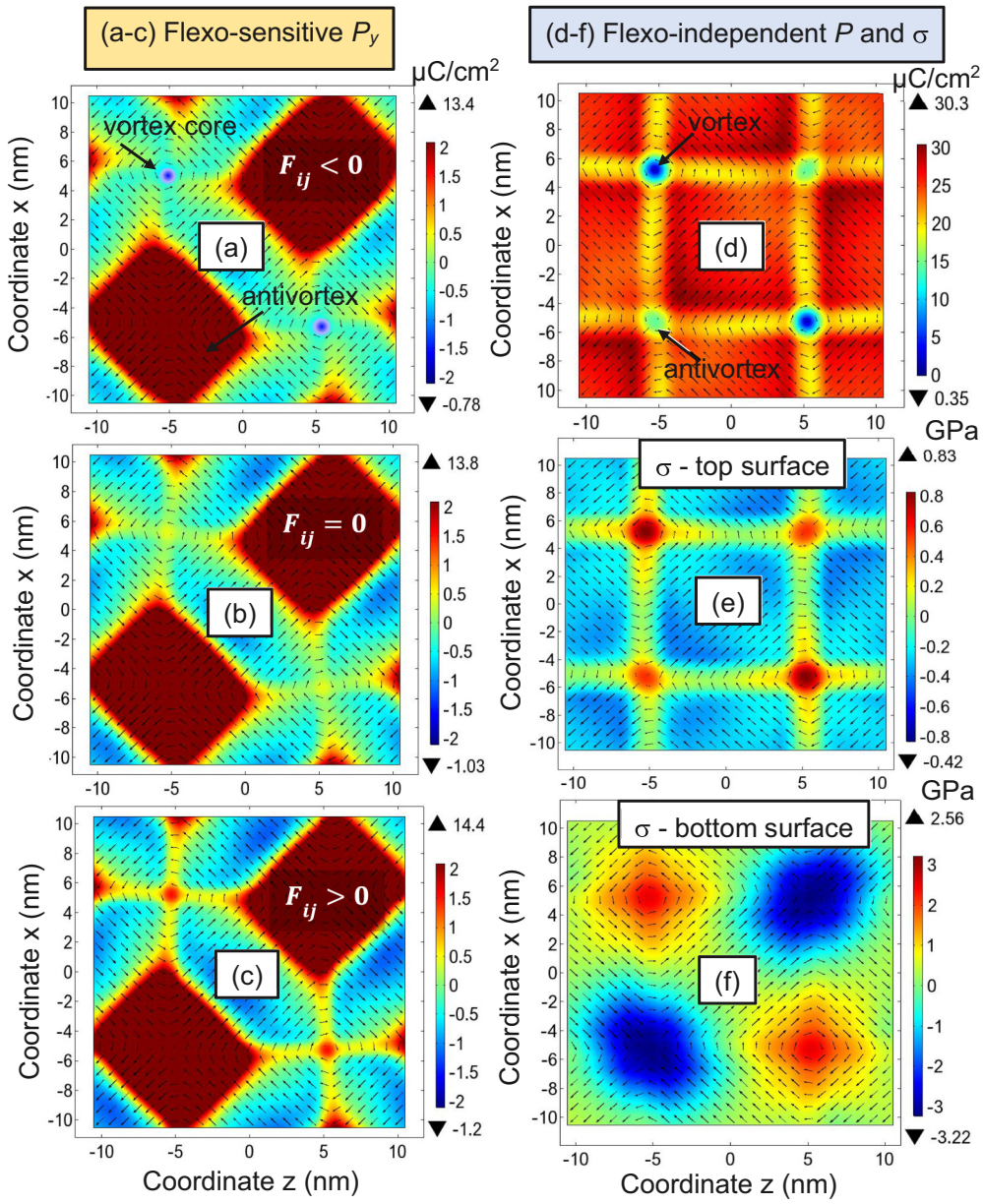

FIG. 3. The XZ sections of the polarization out-of-plane component P_y at the film top surface calculated for negative (a), zero (b), and positive (c) flexoelectric coefficients F_{ij}. The XZ sections of the polarization magnitude P (d) and hydrostatic stress σ (e), (f), which are almost flexoindependent. Arrows show polarization direction in the vortex-antivortex region. The thickness of $BaTiO_3$ film is 9 nm, mismatch strain $u_m = 0.1\%$, and $T = 300$ K.

of P_y) is controlled by the flexocoupling [compare blue and reddish vortex cores in Figs. 3(a)–3(c) and the quadrupolar areas inside dotted ellipses in Figs. 4(d)–4(f)]. The sign of F_{ij} determines the sign of the polarization and its value in the vortex core, as it is seen from the color images in Figs. 4(d)–4(f), and especially from the y profiles in Figs. 5(d), 5(f), and 5(h) calculated for $F_{ij} < 0$, $F_{ij} = 0$, and $F_{ij} > 0$, respectively. The vortex-core polarization becomes significantly smaller for $F_{ij} = 0$ [see Fig. 5(f)]. At the nominal values of F_{ij} (listed in Table AI of Supplemental Material [56]) the maximal polarization in the vortex core reaches (1–1.5) μC/cm^2, depending on the film surface [see Figs. 5(d), 5(f), and 5(h)]. An axial asymmetry of the quadrupolar core is due to different elastic boundary conditions at the mechanically free top surface, where the normal stress is absent, and at the bottom surface clamped to a rigid substrate with a mismatch strain. The asymmetry is clearly seen by comparing the small and high-contrast reddish part with the smooth and more extended blue part of the quadrupolar core in Figs. 4(d) and 4(f), as well as from the comparison of solid and dashed curves in Figs. 5(d) and 5(h). Remarkably, the transformation $F_{ij} \to -F_{ij}$ inverts the vortex core ($P_y \to -P_y$) with respect to the y axis.

In general, the difference in the behavior of the antivortex and vortex cores [shown in Figs. 3(a)–3(c) and Fig. 4] can be explained by the difference of elastic fields in the regions. The hydrostatic stress, $\sigma = \sigma_{11} + \sigma_{22} + \sigma_{33}$, shown in Fig. 3(e) (at the film top surface) and Fig. 3(f) (at the film bottom surface), and in Fig. B3 (at both surfaces), is well localized in the an-

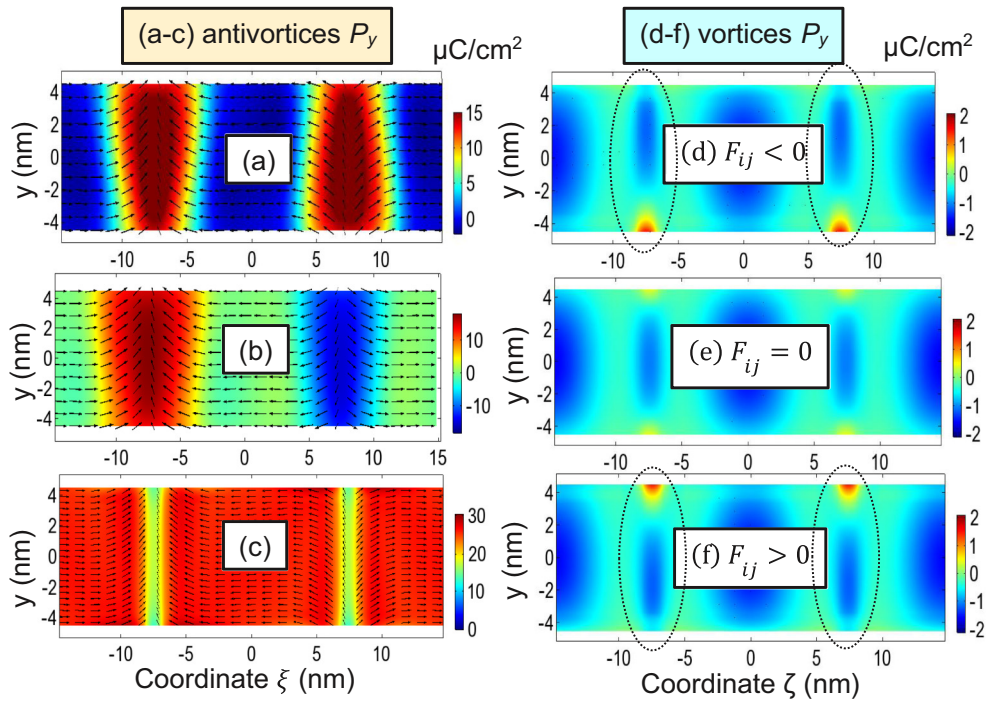

FIG. 4. The ξY sections of the out-of-plane polarization component P_y for different seedings (a), (b) and the magnitude P (c), which are almost flexoindependent. Flexosensitive ζY sections of the P_y calculated for negative (d), zero (e), and positive (f) flexoelectric coefficients F_{ij}. Coordinates $\xi = (x+z)/\sqrt{2}$ and $\zeta = (x-z)/\sqrt{2}$. Arrows in the plots (a)–(c) show polarization direction. The thickness of $BaTiO_3$ film is 9 nm, mismatch strain $u_m = 0.1\%$, and $T = 300$ K.

tivortex and vortex regions. The stress is maximal and positive in the vortex core at the film top surface. At the surface, the stress in the vortex core is significantly smaller than in the antivortex core. The situation is opposite at the film bottom surface, where σ is maximal and negative in the antivortex region, and it becomes positive and significantly smaller in magnitude in the vortex region. The spatial distribution of the dilatational strain, $u = u_{11} + u_{22} + u_{33}$, is very similar to the stress, and thus not shown here. Although the components of elastic stress and strain are virtually independent of the F_{ij} value, their gradients convoluted with flexoelectric coefficients lead to the flexosensitivity of the vortices.

The behavior of the flexosensitive polarization vortex is qualitatively the same as the flexon-type polarization in cylindrical nanoparticles [52]. We argue that the flexosensitive vortex cores can be interpreted as a manifestation of flexons [52] in thin films. To ascertain this conjecture, a topological index of these structures is calculated and analyzed below.

The topological index $n(y) = \frac{1}{4\pi}\int_S \vec{p}[\frac{\partial \vec{p}}{\partial x} \times \frac{\partial \vec{p}}{\partial z}]dxdz$ [63], where $\vec{p} = \frac{\vec{P}}{P}$ is the unit polarization orientation and the integration is performed over the vortex cross-section $S = \{x, z\}$, quantifies the chirality of the polarization structure. Using the method explained in Appendix D of Ref. [52], the approximate y dependence of the topological index is

$$n(y) \approx -\frac{P_y(x=0,\ y, z=0)}{2P(x=0,\ y, z=0)}. \qquad (2)$$

Similarly to the flexon discussed in Ref. [52], $n(y)$ is a normalized profile of the out-of-plane polarization component, and the coordinate origin is placed in the vortex axis. Note that the expression (2) is an approximation since the distribution of $P_y(x,\ y, z)$ is not fully axially symmetric with respect to the vortex axis. The axial asymmetry appears in the form of a square mesh between the vortices (see, e.g., Fig. 3). Although P_y is nonzero for $F_{ij} = 0$ due to the electrostriction coupling, two Bloch points ($P = 0$) located symmetrically under the film surfaces exist for that case [see Fig. 6(d)]. The depth profile of P_y becomes asymmetric with respect to the film surfaces for $F_{ij} \neq 0$, and only one Bloch point exists in this case [see Fig. 6(e)]. The transformation $F_{ij} \to -F_{ij}$ leads to $P_y \to -P_y$ [compare red and blue curves in Fig. 6(e)]. Hence, the sign of P_y, and so the sign of $n(y)$, is defined by the sign of F_{ij}, since the flexoinduced contribution to the polarization component P_y vastly dominates over the electrostriction contribution. The result corroborates the flexon character [52] of the vortex polarization. The dependence $n(y)$ is shown in Fig. 6(e) for zero, positive, and negative F_{ij}, respectively. Since the value $P(0, y, 0)$ coincides with $|P_y(0,\ y, 0)|$ at the vortex axis, and $P_y(0,\ y, 0) = P(0, y, 0) = 0$ in the Bloch point, the topological index jumps in that point from $-1/2$ to $+1/2$ [red curve in Fig. 6(e)], or from $+1/2$ to $-1/2$ [blue curve in Fig. 6(e)], depending on the F_{ij} sign. This observation is in agreement with the fact that a Bloch point carries a topological charge of magnitude 1. In any case, the value of $n(y)$ is equal to $\pm\ 1/2$ at the film surfaces. The result demonstrates the surface localization of the flexosensitive vortices, similarly to the "edge"

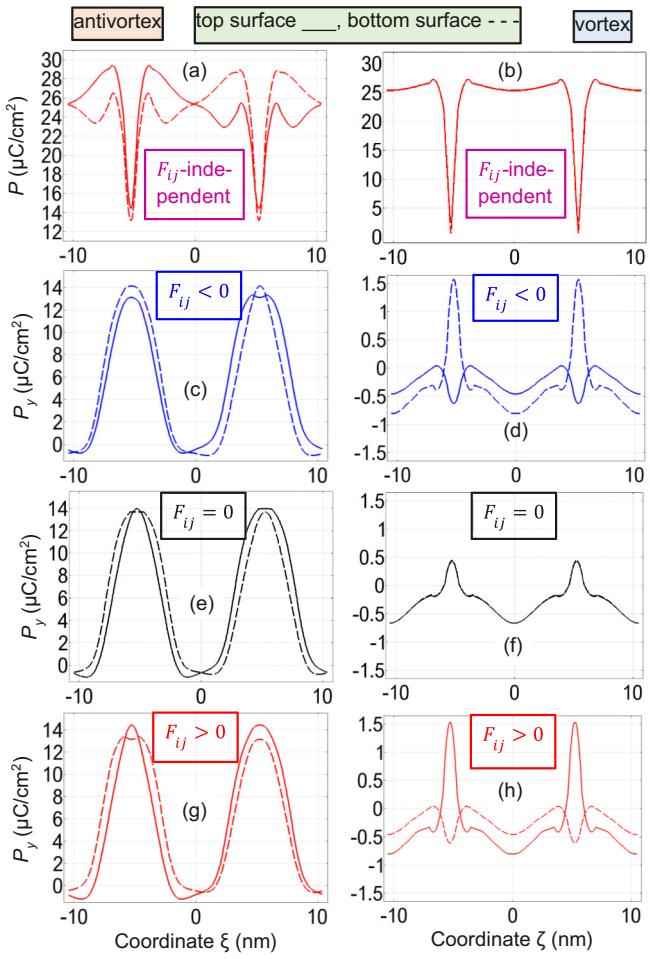

FIG. 5. Profiles of the flexoindependent antivortices (left column) and flexosensitive vortices (right column) at the top (solid curves) and bottom (dashed curves) surfaces of a thin strained $BaTiO_3$ film. (a), (b) Flexoindependent ξ- and ζ profiles of the polarization magnitude P. (c)–(h) Flexosensitive ξ- and ζ profiles of the out-of-plane polarization component P_y for negative (blue curves), zero (black curves), and positive (red curves) flexoelectric coefficients F_{ij}. Coordinates $\xi = (x+z)/\sqrt{2}$ and $\zeta = (x-z)/\sqrt{2}$. The film thickness is 9 nm, mismatch strain $u_m = 0.1\%$, and $T = 300$ K.

localization of flexons in cylindrical nanoparticles [52]. The topological index, which can be interpreted as the degree to which a structure is chiral, changes sign from one surface to the other, and changes sign upon reversal of the sign of F_{ij}. Since $|P_y| \sim |F_{12}|$, the index $n(y)$ increases in magnitude with increasing absolute value of $|F_{ij}|$. These properties make obvious the clear correlation between the flexocoupling and the formation of chiral polar vortices in thin ferroelectric films.

To the best of our understanding, the experiment [46] indicates the possible existence of flexosensitive vortices. However, most phase-field simulations (see, e.g., Ref. [64]) either did not include the flexoelectric effect, or they reveal other trends [49]. Indeed, the flexosensitive vortices are "hidden" by flexoinsensitive antivortices, whose out-of-plane polarization is much higher. Moreover, when we increase the transverse size of the computational cell, the core of the antivortex becomes a complex structure resembling an r-phase domain. Still, the polarization remains strictly vertical in the core region, as for the c-phase domain.

Note that the conditions of the vortex-antivortex structure stability in thin strained films is different from that in nanoparticles due to the 1D spatial confinement in films in comparison with 3D confinement in nanoparticles. In particular, the vortex-antivortex structures can be stable (or at least metastable) in thin films (see, e.g., Ref. [49] and references therein). Moreover, the vortex-antivortex pair can rather annihilate here [59], than transform into a single vortex. Due to the conservation of the winding number as a topological invariant ("+1" for vortex and "−1" for antivortex), vortices and antivortices can annihilate pairwise, leading to a homogeneous state with winding number zero in a process that can be assumed to be continuous and barrierless. The fact that no such annihilation process occurs in the simulations shows that the vortex-antivortex array is energetically stable. We note that multivortex structures and polar skyrmions can be readily stabilized by elastic strains and depolarization effects in ferroelectric films, nanocomposites, and nanodots (see, e.g., Refs. [65,66] and references therein). On the other side, a single vortex can be stable in an electrically open ferroelectric nanoparticle [51,52] and in two interacting ferroelectric nanoparticles [67].

This work, along with earlier [50] and recent [52] studies, predicts different flexosensitive vortexlike states with an axial polarization component in nanosized ferroelectrics of various geometry. Taken together, these findings point towards a general tendency that flexoelectricity can change the topological index (in fact, the skyrmion number) of a ferroelectric vortex.

To define the temperature interval in which the flexosensitive stripes or vortices are stable or metastable, we performed FEM studies of the polarization distribution in the film in the temperature range from 200 to 440 K. A stripe-domain configuration with a flexosensitive out-of-plane polarization component P_y is stable at temperatures lower than 415 K; at higher temperatures it becomes faint as the film transforms to the paraelectric phase.

A vortexlike configuration with a flexosensitive out-of-plane polarization component P_y is metastable at temperatures lower than 400 K (we use the word "metastable" here to underline that the domain stripes have lower energy). The dipolar core of the vortex gradually disappears above 350 K, when the vortex-antivortex structure with cores transforms into a vortex-antivortex structure without cores. Fingerprints of this coreless vortex-antivortex pattern persist up to the paraelectric transition at about 420 K (see Fig. B4 in Appendix B of Supplemental Material [56]). The relatively wide temperature range ($200 < T < 350$ K) of the flexosensitive vortices metastability gives us the hope that the domain morphology can be observed experimentally in thin ferroelectric films by PFM, cAFM [45–47], and nonlinear optical microscopy [48] methods.

The disappearance of antivortex cores when the temperature increases above 320 K is related to the transition from the monoclinic r phase (with all three polarization components) to the orthorhombic a phase (with two in-plane components of polarization). The monoclinic-orthorhombic transition occurs at about 340 K for thick $BaTiO_3$ films with misfit strain

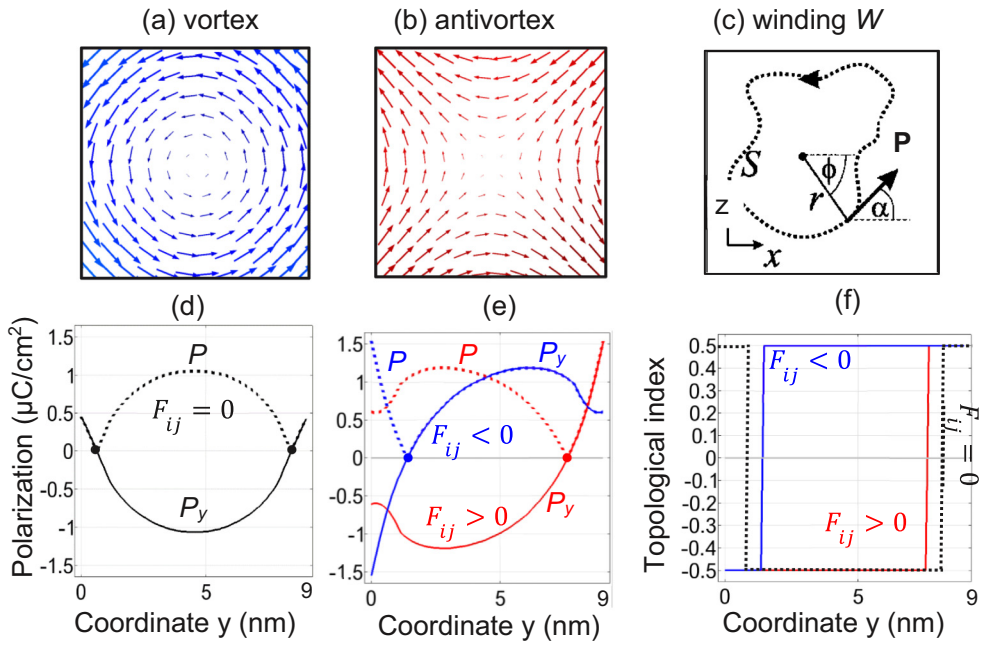

FIG. 6. (a) A ferroelectric vortex ($W = +1$) and (b) antivortex ($W = -1$), whose topology can be distinguished by the winding number W (c). Part (c) is redrawn from Ref. [59]. (d), (e) Depth profiles of the out-of-plane polarization component P_y (solid curves) and magnitude P (dotted curves) calculated at the vortex axis for zero [black curves, (d)], negative [blue curves, (e)] and positive [red curves, (e)] flexoelectric coefficients F_{ij}. Circles are Bloch points, where $P = 0$. (f) The y profile of the polarization's topological index $n(y)$ for zero (black dotted lines), positive (solid red lines), and negative (solid blue lines) F_{ij}. The film thickness is 9 nm, mismatch strain $u_m = 0.1\%$, and $T = 300$ K.

$+0.1\%$ and without dead layers [see dotted lines in Fig. 1(b)], and its temperature decrease to 320 K in thin $BaTiO_3$ films with dead layers is caused by the depolarization field arising from the layers.

IV. CONCLUSIONS

In this theoretical work, we have considered the influence of the flexocoupling on the spatial distribution and the temperature behavior of the ferroelectric polarization for different types of stable domain structures in thin ferroelectric films, such as periodic stripe domains and arrays of vortex-antivortex pairs. Our FEM simulations and analytical calculations reveal that an out-of-plane polarization component can be very sensitive to the flexocoupling for both stripe domains and vortices. However, the influence is rather different. Namely, the flexocoupling significantly increases the amplitude of a small out-of-plane polarization component in the stripe domains. The up or down direction of this out-of-plane component depends on the sign of the flexocoupling coefficients. The vortex has a spikelike quadrupolar core controlled by the flexocoupling, whereas the antivortex has a wide smooth dipolar core, whose shape and other features are weakly insensitive to the coupling.

The origin of the flexosensitive vortex is from the system's tendency to minimize its elastic and gradient energy, while an almost uncharged polarization vortex has a negligibly small electrostatic energy. The topological index of the flexosensitive vortex changes sign from one surface to the other, and changes sign upon reversal of the sign of flexoelectric coefficients. This result demonstrates the surface localization of the flexosensitive vortices, similarly to the edge localization of flexons in cylindrical nanoparticles [52]. All these properties make obvious the clear correlation between the flexocoupling and the formation of chiral polar vortices in thin ferroelectric films. Hence, we can interpret the flexosensitivity of the vortex cores as a variant of the effects that stabilize the recently revealed flexons [52] in thin films. To the best of our knowledge, such flexosensitive vortices have not been revealed in existing nanosized ferroelectrics, although several experiments [46,49] and calculations [50,52] suggest their existence.

The relatively wide temperature range ($200 < T < 350$ K) in which the flexosensitive vortices are metastable gives us confidence that these structures can be observed experimentally in thin ferroelectric films by PFM, cAFM, and nonlinear optical microscopy methods, but we need a specific ferroelectric material, where the sign and the magnitude of flexoelectric coefficients can be controlled. The flexosensitive vortices in the ferroelectric material can become promising objects for advanced cryptography, information storage and processing. However, in available thin films, the PFM observation of the flexosensitive vortices is complicated by the presence of much higher contrast antivortices, which are flexoinsensitive.

ACKNOWLEDGMENTS

The authors are grateful to Dr. Bobby Sumpter for useful remarks and stimulating discussions. This material is based upon work (S.V.K.) supported by the U.S. Department of Energy, Office of Science, Office of Basic Energy Sciences, and performed at the Center for Nanophase Materials Sciences, a U.S. Department of Energy Office of Science User Facility. A portion of FEM was conducted at the Center for Nanophase

Materials Sciences, which is a DOE Office of Science User Facility (CNMS Proposal ID No. CNMS2021-B-00843). A.N.M.'s work is supported by the National Academy of Sciences of Ukraine (the Target Program of Basic Research of the National Academy of Sciences of Ukraine "Prospective basic research and innovative development of nanomaterials and nanotechnologies for 2020–2024," Project No. 1/20-H, State Registration No. 0120U102306). R.H. acknowledges funding from the French National Research Agency through Contract No. ANR-18-CE92-0052 "TOPELEC."

[1] M. D. Glinchuk, A. V. Ragulya, and V. A. Stephanovich, *Nanoferroics* (Springer, Dordrecht, 2013).

[2] J. Hlinka and P. Ondrejkovic, Skyrmions in ferroelectric materials, Solid State Phys. **70**, 143 (2019).

[3] A. Gruverman, M. Alexe, and D. Meier, Piezoresponse force microscopy and nanoferroic phenomena, Nat. Commun. **10**, 1661 (2019).

[4] S. V. Kalinin, Y. Kim, D. Fong, and A. N. Morozovska, Surface-screening mechanisms in ferroelectric thin films and their effect on polarization dynamics and domain structures, Rep. Prog. Phys. **81**, 036502 (2018).

[5] J.-J. Wang, B. Wang, and L.-Q. Chen, Understanding, predicting, and designing ferroelectric domain structures and switching guided by the phase-field method, Ann. Rev. Mater. Res. **49**, 127 (2019).

[6] A. K. Tagantsev, Piezoelectricity and flexoelectricity in crystalline dielectrics, Phys. Rev. B **34**, 5883 (1986).

[7] *Flexoelectricity in Solids: From Theory to Applications*, edited by A. K. Tagantsev and P. V. Yudin (World Scientific, New Jersey, 2016).

[8] J.-C. Tolédano and P. Tolédano, *Landau Theory of Phase Transitions* (World Scientific Publishing Company, Singapore, New Jersey, Hong Kong, 1987).

[9] B. Wang, Y. Gu, S. Zhang, and L.-Q. Chen, Flexoelectricity in solids: Progress, challenges, and perspectives, Prog. Mater Sci. **106**, 100570 (2019).

[10] P. Lukashev and R. F. Sabirianov, Flexomagnetic effect in frustrated triangular magnetic structures, Phys. Rev. B **82**, 094417 (2010).

[11] A. P. Pyatakov and A. K. Zvezdin, Flexomagnetoelectric interaction in multiferroics, Eur. Phys. J. B **71**, 419 (2009).

[12] B. M. Tanygin, Symmetry theory of the flexomagnetoelectric effect in the magnetic domain walls, J. Magn. Magn. Mater. **323**, 616 (2011).

[13] E. A. Eliseev, M. D. Glinchuk, V. Khist, V. V. Skorokhod, R. Blinc, and A. N. Morozovska, Linear magnetoelectric coupling and ferroelectricity induced by the flexomagnetic effect in ferroics, Phys. Rev. B **84**, 174112 (2011).

[14] E. A. Eliseev, A. N. Morozovska, V. V. Khist, and V. Polinger, Effective flexoelectric and flexomagnetic response of ferroics, Solid State Phys. **70**, 237 (2019).

[15] M. S. Majdoub, P. Sharma, and T. Cagin, Enhanced size-dependent piezoelectricity and elasticity in nanostructures due to the flexoelectric effect, Phys. Rev B **77**, 125424 (2008).

[16] E. A. Eliseev, A. N. Morozovska, M. D. Glinchuk, and R. Blinc, Spontaneous flexoelectric/flexomagnetic effect in nanoferroics, Phys. Rev. B **79**, 165433 (2009).

[17] F. Ahmadpoor and P. Sharma, Flexoelectricity in two-dimensional crystalline and biological membranes, Nanoscale **7**, 16555 (2015).

[18] G. Catalan, L. J. Sinnamon, and J. M. Gregg, The effect of flexoelectricity on the dielectric properties of inhomogeneously strained ferroelectric thin films, J. Phys.: Condens. Matter **16**, 2253 (2004).

[19] G. Catalan, B. Noheda, J. McAneney, L. J. Sinnamon, and J. M. Gregg, Strain gradients in epitaxial ferroelectrics, Phys. Rev. B **72**, 020102(R) (2005).

[20] E. A. Eliseev, A. N. Morozovska, C. T. Nelson, and S. V. Kalinin, Intrinsic structural instabilities of domain walls driven by gradient couplings: Meandering antiferrodistortive-ferroelectric domain walls in $BiFeO_3$, Phys. Rev. B **99**, 014112 (2019).

[21] E. A. Eliseev, Y. M. Fomichov, S. V. Kalinin, Y. M. Vysochanskii, P. Maksymovich, and A. N. Morozovska, Labyrinthine domains in ferroelectric nanoparticles: Manifestation of a gradient-induced morphological phase transition, Phys. Rev. B **98**, 054101 (2018).

[22] M. J. Han, E. A. Eliseev, A. N. Morozovska, Y. L. Zhu, Y. L. Tang, Y. J. Wang, X. W. Guo, and X. L. Ma, Mapping gradient-driven morphological phase transition at the conductive domain walls of strained multiferroic films, Phys. Rev. B **100**, 104109 (2019).

[23] Y. Nahas, S. Prokhorenko, J. Fischer, B. Xu, C. Carrétéro, S. Prosandeev, M. Bibes, S. Fusil, B. Dkhil, V. Garcia, and L. Bellaiche, Inverse transition of labyrinthine domain patterns in ferroelectric thin films, Nature (London) **577**, 47 (2020).

[24] W. Ma and L. E. Cross, Flexoelectric effect in ceramic lead zirconate titanate, Appl. Phys. Lett. **86**, 072905 (2005).

[25] W. Ma and L. E. Cross, Flexoelectricity of barium titanate, Appl. Phys. Lett. **88**, 232902 (2006).

[26] D. Lee, A. Yoon, S. Y. Jang, J.-G. Yoon, J.-S. Chung, M. Kim, J. F. Scott, and T. W. Noh, Giant Flexoelectric Effect in Ferroelectric Epitaxial Thin Films, Phys. Rev. Lett. **107**, 057602 (2011).

[27] P. Zubko, G. Catalan, A. Buckley, P. R. L. Welche, and J. F. Scott, Strain-Gradient-Induced Polarization in $SrTiO_3$ Single Crystals, Phys. Rev. Lett. **99**, 167601 (2007).

[28] P. Zubko, G. Catalan, A. Buckley, P. R. L. Welche, and J. F. Scott, Erratum: Strain-Gradient-Induced Polarization in $SrTiO_3$ Single Crystals [Phys. Rev. Lett. **99**, 167601 (2007)], Phys. Rev. Lett. **100**, 199906(E) (2008).

[29] I. B. Bersuker, Pseudo Jahn–Teller effect in the origin of enhanced flexoelectricity, Appl. Phys. Lett. **106**, 022903 (2015).

[30] R. Maranganti and P. Sharma, Atomistic determination of flexoelectric properties of crystalline dielectrics, Phys. Rev. B **80**, 054109 (2009).

[31] I. Ponomareva, A. K. Tagantsev, and L. Bellaiche, Finite-temperature flexoelectricity in ferroelectric thin films from first principles, Phys. Rev. B **85**, 104101 (2012).

[32] J. Hong and D. Vanderbilt, First-principles theory and calculation of flexoelectricity, Phys. Rev. B **88**, 174107 (2013).
[33] M. Stengel, Flexoelectricity from density-functional perturbation theory, Phys. Rev. B **88**, 174106 (2013).
[34] C. E. Dreyer, M. Stengel, and D. Vanderbilt, Current-density implementation for calculating flexoelectric coefficients, Phys. Rev. B **98**, 075153 (2018).
[35] L. Shu, X. Wei, T. Pang, X. Yao, and C. Wang, Symmetry of flexoelectric coefficients in crystalline medium, J. Appl. Phys. **110**, 104106 (2011).
[36] H. Le Quang and Q.-C. He, The number and types of all possible rotational symmetries for flexoelectric tensors, Proc. R. Soc. London, Ser. A: Math., Phys. Eng. Sci. **467**, 2369 (2011).
[37] A. N. Morozovska, E. A. Eliseev, Y. A. Genenko, I. S. Vorotiahin, M. V. Silibin, Y. Cao, Y. Kim, M. D. Glinchuk, and S. V. Kalinin, Flexocoupling impact on the size effects of piezo- response and conductance in mixed-type ferroelectrics-semiconductors under applied pressure, Phys. Rev. B **94**, 174101 (2016).
[38] I. S. Vorotiahin, E. A. Eliseev, Q. Li, S. V. Kalinin, Y. A. Genenko, and A. N. Morozovska, Tuning the polar states of ferroelectric films via surface charges and flexoelectricity, Acta Mater. **137**, 85 (2017).
[39] E. A. Eliseev, I. S. Vorotiahin, Y. M. Fomichov, M. D. Glinchuk, S. V. Kalinin, Y. A. Genenko, and A. N. Morozovska, Defect driven flexo-chemical coupling in thin ferroelectric films, Phys. Rev. B **97**, 024102 (2018).
[40] A. N. Morozovska, E. A. Eliseev, M. D. Glinchuk, L.-Q. Chen, and V. Gopalan, Interfacial polarization and pyroelectricity in antiferrodistortive structures induced by a flexoelectric effect and rotostriction, Phys. Rev. B **85**, 094107 (2012).
[41] A. N. Morozovska, R. K. Vasudevan, P. Maksymovych, S. V. Kalinin, and E. A. Eliseev, Anisotropic conductivity of uncharged domain walls in $BiFeO_3$, Phys. Rev. B **86**, 085315 (2012).
[42] P. V. Yudin, A. K. Tagantsev, E. A. Eliseev, A. N. Morozovska, and N. Setter, Bichiral structure of ferroelectric domain walls driven by flexoelectricity, Phys. Rev. B **86**, 134102 (2012).
[43] E. A. Eliseev, P. V. Yudin, S. V. Kalinin, N. Setter, A. K. Tagantsev, and A. N. Morozovska, Structural phase transitions and electronic phenomena at 180-degree domain walls in rhombohedral $BaTiO_3$, Phys. Rev. B **87**, 054111 (2013).
[44] Y. Gu, M. Li, A. N. Morozovska, Y. i Wang, E. A. Eliseev, V. Gopalan, and L.-Q. Chen, Non-Ising Character of a ferroelectric wall arises from a flexoelectric effect, Phys. Rev. B **89**, 174111 (2014).
[45] P. Maksymovych, A. N. Morozovska, P. Yu, E. A. Eliseev, Y.-H. Chu, R. Ramesh, A. P. Baddorf, and S. V. Kalinin, Tunable metallic conductance in ferroelectric nanodomains, Nano Lett. **12**, 209 (2012).
[46] N. Balke, B. Winchester, W. Ren, Y. H. Chu, A. N. Morozovska, E. A. Eliseev, M. Huijben, R. K. Vasudevan, P. Maksymovych, J. Britson, S. Jesse, I. Kornev, R. Ramesh, L. Bellaiche, L. Q. Chen, and S. V. Kalinin, Enhanced electric conductivity at ferroelectric vortex cores in $BiFeO_3$, Nat. Phys. **8**, 81 (2012).
[47] R. K. Vasudevan, A. N. Morozovska, E. A. Eliseev, J. Britson, J.-C. Yang, Y.-H. Chu, P. Maksymovych, L. Q. Chen, V. Nagarajan, and S. V. Kalinin, Domain wall geometry controls conduction in ferroelectrics, Nano Lett. **12**, 5524 (2012).
[48] S. Cherifi-Hertel, H. Bulou, R. Hertel, G. Taupier, K. D. H. Dorkenoo, C. Andreas, J. Guyonnet, I. Gaponenko, K. Gallo, and P. Paruch, Non-Ising and chiral ferroelectric domain walls revealed by nonlinear optical microscopy, Nat. Commun. **8**, 15768 (2017).
[49] Q. Li, C. T. Nelson, S.-L. Hsu, A. R. Damodaran, L.-L. Li, A. K. Yadav, M. McCarter, L. W. Martin, R. Ramesh, and S. V. Kalinin, Quantification of flexoelectricity in $PbTiO_3/SrTiO_3$ superlattice polar vortices using machine learning and phase-field modeling, Nat. Commun. **8**, 1468 (2017).
[50] C. Liu, J. Wang, G. Xu, M. Kamlah, and T.-Y. Zhang, An isogeometric approach to flexoelectric effect in ferroelectric materials, Int. J. Solids Struct. **162**, 198 (2019).
[51] E. A. Eliseev, A. N. Morozovska, R. Hertel, H. V. Shevliakova, Y. M. Fomichov, V. Yu. Reshetnyak, and D. R. Evans, Flexo-elastic control factors of domain morphology in core-shell ferroelectric nanoparticles: Soft and rigid shells, Acta Mater. **212**, 116889 (2021).
[52] A. N. Morozovska, R. Hertel, S. Cherifi-Hertel, V. Yu. Reshetnyak, E. A. Eliseev, and D. R. Evans, Chiral polarization textures induced by the flexoelectric effect in ferroelectric nanocylinders, Phys. Rev. B (2021) (in press), arXiv:2104.00598.
[53] N. A. Pertsev, A. G. Zembilgotov, and A. K. Tagantsev, Effect of Mechanical Boundary Conditions on Phase Diagrams of Epitaxial Ferroelectric Thin Films, Phys. Rev. Lett. **80**, 1988 (1998).
[54] L. D. Landau and I. M. Khalatnikov, On the anomalous absorption of sound near a second order phase transition point, Dokl. Akad. Nauk SSSR **96**, 469 (1954).
[55] J. Hlinka, Mobility of ferroelectric domain walls in barium titanate, Ferroelectrics **349**, 49 (2007).
[56] See Supplemental Material at http://link.aps.org/supplemental/10.1103/PhysRevB.104.085420 for calculation details.
[57] J. Hlinka and P. Márton, Phenomenological model of 90-degree domain wall in $BaTiO_3$ type ferroelectrics, Phys. Rev. B **74**, 104104 (2006).
[58] A. K. Tagantsev and G. Gerra, Interface-induced phenomena in polarization response of ferroelectric thin films, J. Appl. Phys. **100**, 051607 (2006).
[59] R. Hertel and C. M. Schneider, Exchange Explosions: Magnetization Dynamics during Vortex-Antivortex Annihilation, Phys. Rev. Lett. **97**, 177202 (2006).
[60] O. Tchernyshov and G.-W. Chern, Fractional Vortices and Composite Domain Walls in Flat Nanomagnets, Phys. Rev. Lett. **95**, 197204 (2005).
[61] K. Shigeto, T. Okuno, K. Mibu, T. Shinjo, and T. Ono, Magnetic force microscopy observation of antivortex core with perpendicular magnetization in patterned thin film of permalloy, Appl. Phys. Lett. **80**, 4190 (2002).
[62] S. Middelhoek, Domain walls in thin Ni–Fe films, J. Appl. Phys. **34**, 1054 (1963).
[63] K. Everschor-Sitte, J. Masell, R. M. Reeve, and M. Kläui, Perspective: Magnetic skyrmions—Overview of recent progress in an active research field, J. Appl. Phys. **124**, 240901 (2018).
[64] B. Winchester, N. Balke, X. X. Cheng, A. N. Morozovska, S. Kalinin, and L. Q. Chen, Electroelastic fields in artificially

created vortex cores in epitaxial $BiFeO_3$ thin films, Appl. Phys. Lett. **107**, 052903 (2015).

[65] S. Prosandeev and L. Bellaiche, Characteristics and signatures of dipole vortices in ferroelectric nanodots: First-principles-based simulations and analytical expressions, Phys. Rev. B **75**, 094102 (2007).

[66] Y. Nahas, S. Prokhorenko, L. Louis, Z. Gui, I. Kornev, and L. Bellaiche, Discovery of stable skyrmionic state in ferroelectric nanocomposites, Nat. Commun. **6**, 8542 (2015).

[67] J. Wang and Y. Su, Stability of polarization vortices within two interacting ferroelectric nanoparticles, Phys. Lett. A **375**, 1019 (2011).